

Chapter 1

Thomas-Fermi studies of pairing in inhomogeneous systems: nuclear and cold atom systems at overflow

Peter Schuck^{1,2} and Xavier Viñas³

¹*Institut de Physique Nucléaire, IN2P3-CNRS, Université Paris-Sud,
F-91406 Orsay-Cédex, France*

²*Laboratoire de Physique et Modélisation des Milieux Condensés, CNRS
and Université Joseph Fourier, 25 Avenue des Martyrs, Boîte Postale
166, F-38042 Grenoble Cedex 9, France*

³*Departament d'Estructura i Constituents de la Matèria and Institut de
Ciències del Cosmos, Facultat de Física, Universitat de Barcelona,
Diagonal 647, E-08028 Barcelona, Spain
schuck@ipno.in2p3.fr*

A novel Thomas-Fermi (TF) approach to inhomogeneous superfluid Fermi-systems is presented and shown that it works well also in cases where the Local Density Approximation (LDA) breaks down. The novelty lies in the fact that the semiclassical approximation is applied to the pairing matrix elements not implying a local version of the chemical potential as with LDA. Applications will be given to the generic fact that if a fermionic superfluid in the BCS regime overflows from a narrow container into a much wider one, pairing is substantially reduced at the overflow point. Two examples pertinent to the physics of the outer crust of neutron stars and superfluid fermionic atoms in traps will be presented. The TF results will be compared to quantal and LDA ones.

1. Introduction

The quantal treatment of pairing in inhomogeneous systems is a notoriously difficult problem. This is especially true for systems containing a large number N of particles as it is usually the case for cold atoms in traps ($N \sim 10^6$)¹ or even for smaller systems if they are deformed as can happen for nuclei. Semiclassical approaches may be very helpful in such cases. The simple and very well known Local Density Approximation (LDA)² is not always applicable because for its validity the condition that the size of the

Cooper pair (coherence length), ξ , must be smaller than a typical length l over which the mean field potential is varying (l is, e.g., the oscillator length in the case of a harmonic potential) is not always fulfilled. We here, therefore, will apply the TF approximation directly to the pairing matrix elements whose evaluation only requires the usual TF condition that the wave lengths involved must be smaller than l^3 . We will show that, indeed, our approach also works for cases where ξ is larger than l where the LDA fails. We will demonstrate this for the BCS approach in this paper.

The physical systems we are interested in concern cold atoms in traps and nuclei, both in so called overflow or drip configurations. For the latter overflow or drip means that there is such a large neutron excess that the selfconsistent mean field container is full up to the edge. In the inner crust of neutron stars where the nuclei form a Coulomb crystal these extra neutrons overflow into the interstitial space and form there a more or less dense neutron gas which also can be superfluid. In the inner crust the nuclei can actually turn into sheets and the neutron gas can form in between the sheets (a so-called lasagne configuration⁴). As a first example we will treat in a schematic model such a slab configuration as is shown in Fig. 1, mostly because the quantal solution is readily available and, therefore, can serve as a test case for the validity of the TF approximation for treating the pairing problem. Indeed, we will find that the TF approach reproduces the quantal solution of the pairing properties, besides some shell fluctuations, very accurately. On the physical side, we point out that at the overflow point pairing can be strongly suppressed. This finding will then also be reproduced with a system where cold atoms are filled into a spherical container consisting of a narrow part at low filling, suddenly going over into a much wider container at higher chemical potentials, as it is displayed in the left panel of Fig. 3⁵. A slightly different situation occurs with a double well potential, as the one shown in the left panel of Fig. 5. Again this potential is used in a slab configuration and TF and quantal results for the gaps are compared.

At the end, we return to nuclei in the crust of neutron stars where they are embedded in a more or less dense gas of neutrons. A Wigner-Seitz cell approximation will be applied to investigate this situation. Again similar features as in the previous examples will be found around the overflow point in the transition from the outer to the inner crust.

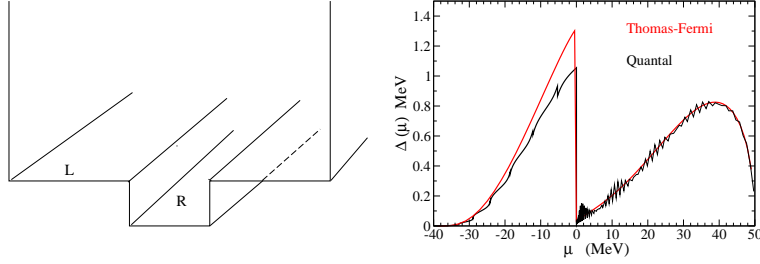


Fig. 1. Left: Schematic view of the slab used in this work with a perspective view of the potential which is translationally invariant in x, y direction. Right: Quantal and TF pairing gaps in the slab geometry as a function of the chemical potential.

2. The formalism

In this section, we will explain the TF approach to the pairing problem and apply it first to the slab configuration shown in Fig. 1. Let us start out by writing down the usual BCS equations in three dimensions

$$\Delta_\nu = - \sum_{\nu'} V_{\nu, \nu'} \frac{\Delta_{\nu'}}{2\sqrt{(\varepsilon_{\nu'} - \mu)^2 + \Delta_{\nu'}^2}}, \quad (1)$$

where the ε_ν 's are the single particle energies and μ the chemical potential which can be used to fix the particle number $N = \sum_\nu v_\nu^2$ with

$$v_\nu^2 = \frac{1}{2} \left[1 - \frac{\varepsilon_\nu - \mu}{\sqrt{(\varepsilon_\nu - \mu)^2 + \Delta_\nu^2}} \right]. \quad (2)$$

The wave functions and eigenenergies of a box as shown in Fig. 1 with a potential-hole are given in⁶. For pairing, we use a contact force with a cut off Λ , to make things simple. The single particle states in a slab configuration then become $|\nu\rangle = |n, \mathbf{p}\rangle$ where n are the discrete quantum numbers in transverse direction and \mathbf{p} the momentum quantum numbers in slab direction. To obtain the gap equation in this case we start by integrating the gap equation (1) over momenta in slab direction:

$$\Delta_n = - \sum_{n'} \int \frac{d^2 p}{(2\pi\hbar)^2} V_{nn'} \Theta(\Lambda - \varepsilon_{n'} - \varepsilon_p) \frac{\Delta_{n'}}{2E_{n'}(p)}, \quad (3)$$

with $E_n(p) = \sqrt{(\varepsilon_n + \varepsilon_p - \mu)^2 + \Delta_n^2}$ the quasiparticle energy, $\Theta(x)$ the step function, and $\varepsilon_n, \varepsilon_p$ being the discrete single particle energies in transverse direction and kinetic energies in slab direction, respectively. After simple algebra, one arrives at the following gap equation for a slab configuration

$$\Delta_n = - \sum_{n'} \Theta(\Lambda - \varepsilon_{n'}) V_{nn'} K_{n'}. \quad (4)$$

The pairing tensor in equation (4) is then given by

$$K_n = \frac{m}{4\pi\hbar^2} \Delta_n \ln \frac{\Lambda - \mu + \sqrt{(\Lambda - \mu)^2 + \Delta_n^2}}{\varepsilon_n - \mu + \sqrt{(\varepsilon_n - \mu)^2 + \Delta_n^2}}, \quad (5)$$

where m is the particle mass and the indices n stand for the level quantum numbers in the confining potential of the left panel of Fig. 1. The matrix elements $V_{nn'} = -g \int_{-L}^{+L} |\varphi_n(z)|^2 |\varphi_{n'}(z)|^2 dz$ of the pairing contact force $v_{pair}(\mathbf{r} - \mathbf{r}') = -g\delta(\mathbf{r} - \mathbf{r}')$ used in this case can be evaluated straightforwardly from the wave functions $\varphi_n(z)$ given in⁶.

Before we show the results, let us explain our Thomas-Fermi (TF) approach for this problem. In the weak coupling regime, we have $\Delta/\mu \ll 1$. In this case the canonical basis⁷ can be replaced by the Hartree-Fock or mean-field one:

$$H|n\rangle = \epsilon_n|n\rangle. \quad (6)$$

At equilibrium and for time reversal invariant systems canonical conjugation and time reversal operation are related by

$$\langle \mathbf{r} | \bar{n} \rangle = \langle n | \mathbf{r} \rangle \Rightarrow \langle \mathbf{r}_1 \mathbf{r}_2 | n \bar{n} \rangle = \langle \mathbf{r}_1 | \hat{\rho}_n | \mathbf{r}_2 \rangle, \quad (7)$$

with $\hat{\rho}_n = |n\rangle\langle n|$. For the pairing matrix element, we, therefore, can write

$$V_{nn'} = \langle n \bar{n} | v | n' \bar{n}' \rangle = \int \langle \mathbf{r}_2 | \hat{\rho}_n | \mathbf{r}_1 \rangle \langle \mathbf{r}_1 \mathbf{r}_2 | v | \mathbf{r}'_1 \mathbf{r}'_2 \rangle \langle \mathbf{r}'_1 | \hat{\rho}_{n'} | \mathbf{r}'_2 \rangle d\mathbf{r}_1 d\mathbf{r}_2 d\mathbf{r}'_1 d\mathbf{r}'_2. \quad (8)$$

The Schroedinger equation (6) can be written in terms of $\hat{\rho}_n$ as

$$(H - \epsilon_n) \hat{\rho}_n = 0. \quad (9)$$

Taking the Wigner transform of this latter equation, we obtain in the $\hbar \rightarrow 0$ limit the following c-number equation⁷: $(H_{cl.} - \epsilon) f_\epsilon(\mathbf{R}, \mathbf{p}) = 0$. The

solution of this equation in the sense of distribution theory is with $x\delta(x) = 0$ given by

$$f_E(\mathbf{R}, \mathbf{p}) = \frac{1}{g^{TF}(E)} \delta(E - H_{cl.}) + O(\hbar^2). \quad (10)$$

with

$$H_{cl.} = \frac{p^2}{2m^*(\mathbf{R})} + V(\mathbf{R}) \quad \text{and} \quad g^{TF}(E) = \frac{1}{(2\pi\hbar)^3} \int d\mathbf{R} d\mathbf{p} \delta(E - H_{cl.}).$$

with $m^*(\mathbf{R})$ the effective mass and $V(\mathbf{R})$ the mean field potential. Equation (10) means that the phase space distribution corresponding to a state $|n\rangle$ at high energy is concentrated around the classical energy shell that, indeed, is a well known fact.

The TF version of the gap equation (4) then reads

$$\Delta(E) = - \int_{V_0}^{\Lambda} dE' g(E') V(E, E') K(E') \quad (11)$$

with $K(E)$ an obvious generalisation of K_n in (5). The matrix elements $V(E, E')$ can be evaluated in replacing $|\varphi_n(z)|^2$ by³

$$\rho_E^{TF}(z) = \int \frac{dp}{2\pi\hbar} f_E(z, p) = \frac{1}{g^{TF}(E)} \frac{1}{2\pi} \left(\frac{2m}{\hbar^2}\right)^{1/2} [E - V(z)]^{-1/2}, \quad (12)$$

which is the on-shell TF density in transverse direction (please note that we are in a 1D case here, contrary to what is treated above where it is 3D). As the reader will easily realise, the way of proceeding is very different from usual LDA where the finite size dependence is put into the (local) chemical potential, $\mu(z) = \mu - V(z)$, whereas here it is put into the matrix elements of the pairing force (notice that in LDA they are computed using plane wave functions).

3. Results

We are now in a position to solve the quantal and TF gap equations in the slab geometry for the confining potential displayed in the left panel of Fig. 1. As an example we take as cut off $\Lambda = 50$ MeV counted from the edge of the pocket potential whose depth be $V_0 = -40$ MeV. Its extension ranges from $-R$ to $+R$ with $R = 10$ fm. The wide potential with infinitely

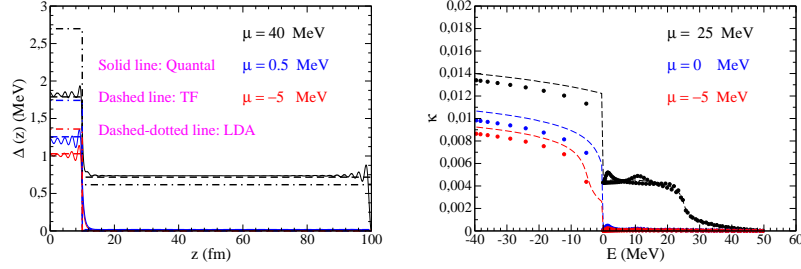


Fig. 2. (Coloronline) Left panel: Position dependence of the gap in the slab geometry for different values of the chemical potential. Quantal, TF, and LDA results are shown. Notice that Δ for $\mu = 0.5$ and -5.0 MeV is practically zero in the gas region. Right panel: Comparison of quantal (dots) and TF (broken lines) values of the pairing tensor K .

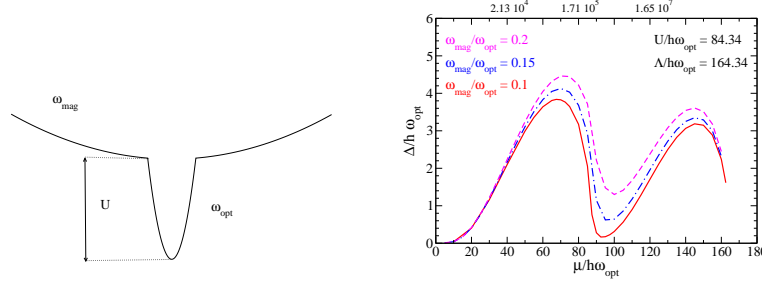


Fig. 3. (Coloronline) Average TF gaps at the Fermi energy as a function of the chemical potential (right panel) for the potential shown in the left panel. In the completely filled optical trap ($\mu = U$) we accommodate 10^5 atoms in each spin state. The total number of atoms in the trap with $\mu/h\omega_{opt}=40, 80$ and 120 are indicated in the upper horizontal axis.

high walls has extension from $-L$ to $+L$ with $L = 100$ fm. For the coupling strength we take $g = 150$ MeV fm³. The result for the gap at the chemical potential μ is shown in the right panel of Fig. 1 as a function of μ . We start with μ from the bottom of the pocket well, i.e. with zero density. We then increase μ , i.e. the density. We see that once the fill up of the pocket reaches its top, the values of the gap sharply drop and practically reach zero. In the continuum the gaps slowly rise again. We see that quantal and TF values are in close agreement. The overshoot of the TF solution for negative μ very likely is due to the smallness of the pocket

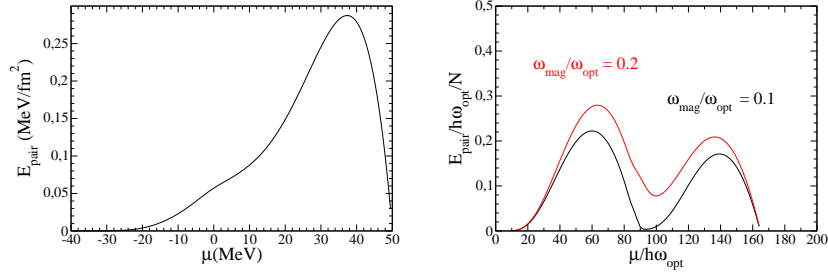


Fig. 4. (Coloronline) Pairing energy as a function of the chemical potential for the slab (left panel) and the double harmonic potential discussed in the text (right panel).

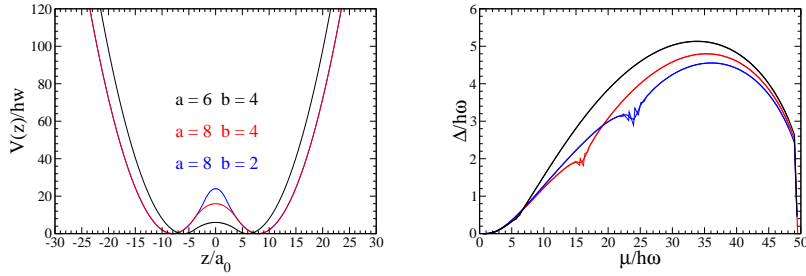


Fig. 5. (Coloronline) Double well potential in slab geometry (left) and gaps as a function of the chemical potential (right). The different curves correspond to the parameters $a=6$ and $b=4$, $a=8$ and $b=4$ and $a=8$ and $b=2$ (see text for explanation). Please note that TF and quantal values cannot be distinguished on the scale of the figure, besides in the region of the dips where TF passes through the average of the quantal oscillations.

which only can accommodate nine bound levels. The bunches of resonances in the continuum of the quantal solution are interesting but we did not try to explain them in this work. Before we come to an explanation of the drop of the gaps at overflow (drip), let us study the gaps as a function of position in transverse direction. Quantally the position dependent gap is defined as: $\Delta(z) = -gK(z)$ with $K(z) = \sum K_n |\varphi_n(z)|^2$. Semiclassically, the relation between the gap and the pairing tensor becomes:

$$\Delta(z) = -g \int_{V_0}^{\Lambda} dE g^{TF}(E) K(E) \rho_E^{TF}(z). \quad (13)$$

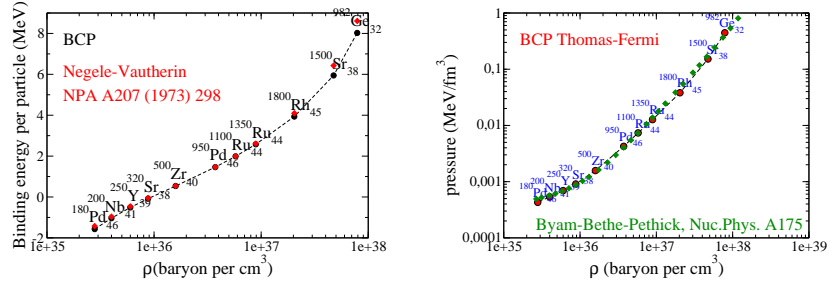


Fig. 6. (Coloronline) Left: Binding energies per particle as a function of average density in a Wigner-Seitz cell. Red dots indicate quantal Skyrme HF calculations by Negele-Vautherin and black dots correspond to semiclassical results with the variational Wigner-Kirkwood (VWK) method and the Gogny D1S force. Right: BCP equation of state for the inner crust compared with the predictions of the Baym-Bethe-Pethick one.

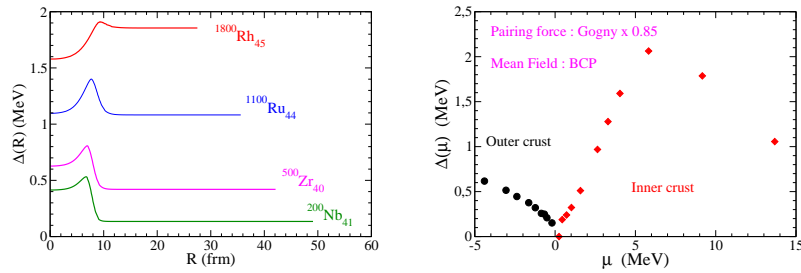


Fig. 7. (Coloronline) Left panel: Radial dependence of the TF gaps in the considered WS cells. The end points indicate the radius of the WS cells. Right panel: Gap values for the Wigner-Seitz cells corresponding to Fig. 6. The zero point indicates the transition from isolated nuclei (black dots) to the dripped case (red diamonds).

In the left panel of Fig. 2, we show the gap profiles for three different values of the chemical potential: $\mu = 40, 0.5$, and -5 MeV. We see that quantal and TF results agree, up to shell fluctuations, very well. We also show the LDA results. They can be locally as wrong as by 50 percent. For other choices of system parameters the LDA error may even be worse. This stems from the fact that in TF (and, of course, also quantally), there is coupling between inside and outside the pocket, i.e. the Cooper pair wave function extends into both regions what tends to equilibrate the values of the gaps. In LDA the contrast is much too strong. The drop of the gaps

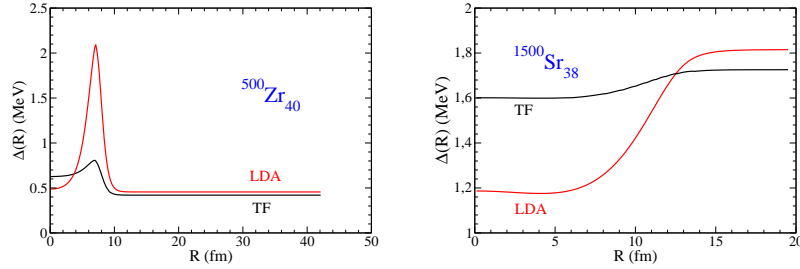


Fig. 8. (Coloronline) Comparison between TF and LDA gaps as a function of the position in a WS cell containing a single $^{500}_{40}\text{Zr}$ nucleus (left) and $^{1500}_{38}\text{Sr}$ (right).

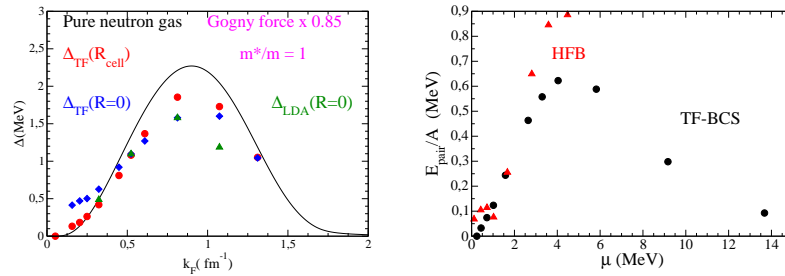


Fig. 9. (Coloronline) Left panel: The TF (blue diamonds) and LDA (green triangles) gaps at the origin are compared with the gaps of the free neutron gas ($\Delta(R_{cell})$, red dots) as a function of the Fermi momentum of the neutron gas at the edge of the cell. Right panel: pairing energy per nucleon in the inner crust. The TF results are compared with the quantal HFB values of ref.²¹

when crossing the threshold can be explained by the fact that the single particle states are strongly delocalised in the outer container and, thus, their contribution to the pairing matrix element $V_{n,n'}$ becomes very small. In the right panel of Fig. 2 we show the quantal and TF pairing tensors, K_n and $K(E)$ respectively, defined before. We emphasize again the close agreement between quantal and TF results.

Having gained faith into our TF approach, we now can explore other geometries and other systems, which are more difficult for quantal solutions. In the right panel of Fig. 3 we display the result for the gap Δ in

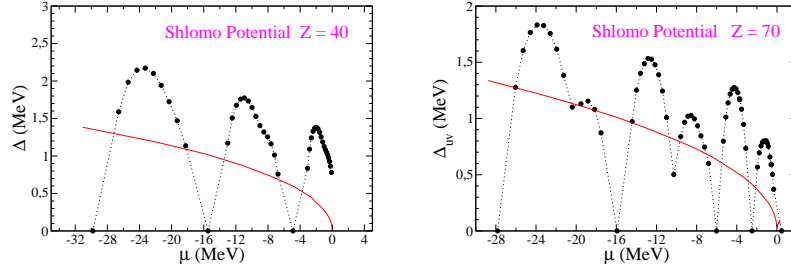


Fig. 10. (Coloronline) Neutron pairing gaps averaged with the pairing tensor (uv) along the $Z=40$ and $Z=70$ isotopic chains obtained with the Shlomo potential as mean field and the finite range Gogny force renormalized by an attenuation factor of 0.85 in the pairing channel. Filled dots correspond to the BCS calculation and solid thick lines to the TF approach.

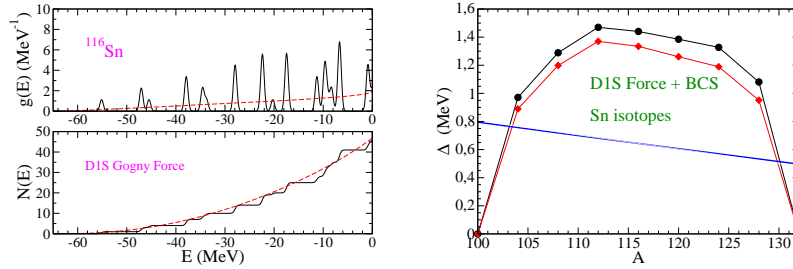


Fig. 11. (Coloronline) Left: TF (dashed line) and fluctuating (solid line) level density (upper panel) and accumulated level density (lower panel). See text for details. Right: Averaged gaps along the Sn isotopic chain computed fully quantally at BCS level using the Gogny D1S force (circles), semiclassically using the fluctuating level density (diamonds), and with the TF approach (solid line).

the spherical double harmonic oscillator potential shown in the left panel of Fig. 3. The latter may be realised with cold fermionic atoms to study the overflow situation. A zero range pairing force with strength $g=-1.0$ and cut off $\Lambda=164.34$ (in the corresponding optical trap units with $\omega_{opt} = 2\pi \times 1000$ Hz taken from⁸) is used in this case. We see that the result is qualitatively similar to the slab case, though in this spherical geometry the dip does not quite reach zero and also is shifted slightly to an energy above the break point of the potential. Note that this depends strongly on the choice of the ratio $\omega_{mag}/\omega_{opt}$ as it can be seen in the figure. Also the gap starts to de-

crease towards the minimum quite early. This is contrary to what happens in the slab case, where the change is very abrupt. The reason probably lying in the spherical symmetry of the considered system. It would be interesting to see whether our prediction can be verified experimentally.

It also is interesting to study the pairing energy, defined in TF approximation as $E_{pair} = \frac{1}{N} \int dE g(E) \Delta(E) \kappa(E)$. The results of the pairing energy per particle for the slab potential, Fig. 1, and in the H.O. case of Fig. 3 are shown in Fig. 4. We see that E_{pair} behaves quite differently in the two cases. In the spherical example for cold atoms the depression at the overflow point is also seen in the pairing energy whereas the depression is completely washed out in the case of the slab. The reason for this qualitative and strong difference must come from the fact that in the slab case the drop of the gap as a function of the chemical potential $\Delta(\mu)$ at overflow is extremely steep, almost vertical. Furthermore, in the pairing energy corresponding to the slab, the pairing tensor $\kappa(E)$ should actually be replaced by $K(E)$ corresponding to (5). Being integrated over the momenta in slab direction it does not show any peak at $E = \mu$ as is the case in the spherical case. Therefore, in the integral of E_{pair} also gap values further away from the overflow point are picked up which are not small at all.

Another interesting geometry which can be considered is a potential with a barrier at the origin, i.e. a double well potential, see the left hand panel of Fig. 5. We treat this example again in slab geometry as in Fig. 1. It roughly may mock up an oblate and very elongated trap potential for cold atoms with a double well potential in transverse direction. The results for the gaps $\Delta(\mu)$ are shown in the right hand panel of Fig. 5. This potential, which depends on two parameters a and b , is defined as follows: $V(z) = \frac{1}{2}(z+a)^2$ if $z \leq b$, $V(z) = \frac{a(a-b)}{2} + \frac{1}{2}(1 - \frac{a}{b})z^2$ when $|z| \leq b$ and $V(z) = \frac{1}{2}(z-a)^2$ for $z \geq b$. As before, TF and quantal results are in excellent agreement. When the chemical potential reaches the top of the barrier, there occurs again a reduction of the gaps, since the wave functions at the Fermi surface suddenly get more extended above the barrier. This is the same effect as in the previous examples, although it is in this case less pronounced. Such a double well potential allows for the creation of a Josephson current if the population in left and right well are out of balance.⁹ Our TF approach may strongly facilitate the description of this phenomenon in the case of cold fermionic atoms.

Let us now make a more realistic study of Wigner-Seitz (WS) cells to simulate the inner crust of neutron stars. In this approach one considers a single nucleus of N neutrons and Z protons inside a spherical box of radius R_{cell} as well as a uniform background of Z electrons to preserve the charge neutrality of the cell⁴. The mean-field, as explained in¹⁰, is computed selfconsistently in the TF approach using the BCP energy density functional¹¹. In this semiclassical calculation we consider the same WS cells and mass numbers as in the old quantal calculation of Negele and Vautherin¹². However, as far as shell corrections are not included, in our semiclassical calculation, we take as representative nucleus in each cell, the beta-stable one computed à la TF along the corresponding isotopic chain. This is why the atomic numbers Z of the representative nuclei differ from the ones reported in¹² while their mass numbers A coincide.

It must be pointed out that the total energy per baryon obtained with our TF approach is in very good agreement with the quantal values reported in¹², as it is explicitly discussed in Ref.¹⁰ and again shown here in the left panel of Fig. 6. As an additional test of our TF mean-field calculation, in the right panel of Fig. 6, we also display the EOS (i.e. pressure as a function of the WS average density) in the inner crust obtained in our semiclassical calculation compared with the results provided by the Baym-Bethe-Pethick EOS¹³ which is considered a benchmark in large scale neutron star calculations. We find excellent agreement between both calculations.

The semiclassical description of the WS cells including pairing correlations at TF level is obtained from this mean-field using the finite range part of the Gogny D1S force¹⁴ in the pairing channel¹⁵. In the left panel of Fig. 7, we display the radial dependences of the gaps in some selected WS cells. It is seen that when the gap is small outside the region of the nucleus, then the gap also is small inside the nucleus. This stems from the very large coherence length where one neutron of a Cooper pair can be in the huge volume of the gas and the other inside the small volume of the nucleus (proximity effect). In this way the gas imprints its behavior for the gap also inside the nucleus. Such a conclusion was also given in a quantal Hartree-Fock-Bogoliubov (HFB) calculation by Grasso et al. in¹⁶ what shows that the here employed BCS approximation apparently yields very similar answers as a full HFB calculation for WS cells¹⁷⁻¹⁹. More precisely, let us point out that the gaps in the region of the nuclei, corresponding to the inner crust and displayed in this figure, are strongly affected by the neutron gas. To illustrate this fact, we display in the right panel of Fig. 7 the values of $\Delta(R=0)$ (blue diamonds) and $\Delta(R=R_{cell})$ (red filled cir-

cles), compared with the gaps of the free neutron gas (continuous black line) at the density corresponding to the edge of the cell $\rho(R_{cell})$. The semiclassical TF gaps $\Delta(R = R_{cell})$, as expected, closely follow the free neutron gas values in agreement with HFB calculations¹⁹. As seen, the gap values at the origin, $\Delta(R = 0)$, are also strongly correlated with the gaps of the free neutron gas. For small average densities below $\rho \sim 0.02 \text{ fm}^{-3}$, the $\Delta(R = 0)$ values are larger than the corresponding gaps at the edge of the WS cell, as it can also be appreciated in the left panel of the figure. However, for larger values of the average density in the WS cell, this tendency is reversed and the gap at the edge is larger than at the origin pointing to the increasing influence of the neutron gas. These conclusions can also be drawn from an independent quantal study in Ref.²⁰ where in the right panel of Fig. 4 very similar features for the local gap values in different WS cells can be seen as in our TF study. We also show in Fig. 7, right panel, the LDA values of $\Delta(R = 0)$ by the filled (green) triangles. We remark that those values undershoot quite strongly the corresponding TF values at the higher densities.

For further illustration of this effect, we show in the two panels of Fig. 8 a comparison between LDA and present TF results for the gaps in two particular WS cells. In the case of the largest cell whose representative nucleus is $^{500}_{40}\text{Zr}$, we see locally a huge difference in the surface region of the nucleus. This simply stems from the fact that in this case the gap is very small and, therefore, the coherence length very large invalidating LDA. A study with examples a little less unfavorable for LDA is given in²². This wrong behaviour of the local LDA gaps at low average densities can also be seen in Fig. 6 of Ref.¹⁸. From that figure we conclude that our TF calculation reproduces, qualitatively, the global trends of the quantal gaps at low average densities. The behaviour of the semiclassical gaps at high average density is clearly different and it is dominated by the neutron gas as it can be seen in the right panel of Fig. 8 where the gap of the representative nucleus $^{1500}_{38}\text{Sr}$ is plotted as a function of the radius. Locally, LDA and TF show a depression in the center and the gap increases with increasing distance till it reaches its neutron gas value. The central depression is stronger by about 30 percent in LDA than in TF. This behaviour is similar to the one exhibited by the quantal gaps compared with the LDA ones displayed in Ref.²³. In other words, this means that the contrast between inside and outside of the nucleus is much too pronounced in LDA, however, quantally as well as in TF this contrast is strongly attenuated by the proximity effect. The semiclassical TF gaps

at the Fermi level are displayed in the left panel of Fig. 9 as a function of chemical potential μ . In the inner crust, i.e. for positive values of μ , they show a similar behaviour as the gaps at the edge of the WS cell displayed in the right panel of Fig. 7. This behaviour can be expected as far as the gap at the Fermi level is rather an average quantity and, therefore, strongly influenced by the neutron gas as it also happens in the HFB calculations of Ref.¹⁹. In this figure we also include the gaps of some WS cells corresponding to the outer crust where all neutrons are bound with negative values of the chemical potential μ . Again we see that the gap practically vanishes at zero chemical potential when the neutrons start to drip. In the right panel of Fig. 9 we display the pairing energies per nucleon corresponding to the WS cell of the inner crust. These energies are also correlated with the neutron gas and display a similar behaviour as the one of the gaps at the Fermi energy. Again the pairing energy per nucleon vanishes when neutrons arrive at the drip. It is rewarding that in the low average density regime the TF pairing energies per nucleon follow the same trend as the quantal HFB ones²¹ shown by the (red) filled triangles (however, a slightly different model with a somewhat stronger pairing force than in our case is used there).

For isolated nuclei at the neutron drip the situation may be somewhat different. First, it may be that in this situation the difference between HFB and BCS approaches is more significant. Also strong shell fluctuations surely play an important role. Somewhat conflicting results in this respect exist in the literature. In ref²⁴ very similar results to ours are found for *S*-wave pairing, see Fig. 4 of this reference and also the discussion about it in²⁵. On the other hand in²⁶ the gap seems to rise towards the drip before it bends down. Similar results have also been found in²⁷. The HFB calculation of Hamamoto has recently been repeated and extended passing from negative chemical potentials to positive ones and it was found that the *S*-wave gap clearly continues down to zero, touching zero at a slightly positive value of μ ²⁸. In explaining why in other works the gap is rising towards the drip, one has to keep in mind that an average gap should be calculated with the pairing tensor and *not* with the density matrix. The latter picks up the gaps at all energies which may not be small at all, even though the gap at the Fermi level is very small, see the right panel of Fig. 1. On the other hand an average with the pairing tensor generally only picks up the (small) gaps around the Fermi level. It also is intuitively clear that for other than *S*-waves gaps the situation will be somewhat different. This is due to the finite centrifugal barrier which keeps

the wave function concentrated on the domain of the nucleus as long as the corresponding energy stays below the barrier. However, large scale HFB calculations around the neutron drips of nuclei indicate that in general pairing is reduced at the drip line.²⁹ In Fig. 10 we show a schematic study which may qualitatively reflect the real situation. A Z, N dependent Woods Saxon potential (without spin orbit) given by Shlomo³⁰ was taken as the mean field and the BCS equation has been solved with the Gogny D1S pairing force^{14,15}. Isotopic chains for two values of Z have been calculated. For $Z = 70$ the drip practically coincides with a shell closure of the neutrons and, therefore, the gap falls to zero at the drip for this case. On the other hand, for $Z = 40$ the neutron drip does not coincide with a closed shell and then the gap has substantial values around the drip. Globally, however, a clear decreasing tendency of the gap towards the neutron drip can be observed as also reflected by the TF values. The fact that neutron gaps decrease with increasing isospin was actually pointed out long time ago, see Refs.^{31,32}. Real nuclei at the neutron drip may be either spherical or deformed (see Ref.³³). For spherical drip nuclei it often happens that neutrons are at or very close to shell closure whereas for deformed nuclei this is not the case. The two situations then resemble the scenario displayed in the right and left panels of Fig. 10 though, there, we imposed sphericity also for the case $Z = 40$.

A very promising possibility to recover shell effects is given by the fact that the latter mostly stem from the shell effects in the level density. We have discussed this problem with some detail in an earlier publication³⁴. The basic idea is to replace in the TF gap equation (6) the semiclassical $g(E)$ by its quantal counterpart, slightly smeared out by using gaussians centered at the quantal eigenvalues so that one obtains a continuous function of E without destroying substantially the shell structure as is shown in Fig. 11. Inserting this into the gap equation (6), allows to recover almost completely the full quantal gaps as is shown in the right panel of Fig. 11.

In this work, we exclusively have treated pairing in BCS approximation. However, for certain situations and quantities, the more general HFB approach may be mandatory as, e.g., in the cases of rotation or a magnetic field. It is relatively straightforward to generalise the BCS-TF approach also to the HFB case. For this one has to consider fully non diagonal matrix elements $\langle n_1 n_2 | v | n_1' n_2' \rangle$. In the matrix elements, we have replaced $|\varphi_n(z)|^2$ by the TF expression for the on shell density $\rho_E^{TF}(z)$. In the off diagonal pairing matrix element, we need wave functions and not densities.

Therefore, in TF approximation, we then can use $\varphi_n(z) \rightarrow \sqrt{\rho_E^{TF}}(z)$ for the individual wave functions. Of course, this complicates the solution of the gap equation but this is always the price to pay when passing from BCS to HFB, quantally as well as semiclassically. The TF-HFB approach shall be investigated in future work³⁵. Let us finally mention that for spherical systems the TF approach can be generalised to partial waves as was done for the pairing matrix elements in³.

4. Summary

Summarizing, we have studied superfluid fermions in a large container, either external (cold atoms) or created self consistently (nuclei) for situations where the top of the fluid reaches the edge of a small pocket located at the origin of the wide confining potential. The gap drops to zero at the edge before rising again when the density fills up the outer container. This at first somewhat surprising phenomenon can be explained quite straightforwardly. Such situations, as already mentioned, can exist in cold atoms and nuclei in the inner crust of neutron stars, two examples treated here with their specific form of containers. For small systems, like isolated nuclei at the neutron drip, the situation may be blurred by shell effects.

As an important second aspect of this work, we showed that a novel Thomas-Fermi approach to inhomogeneous situations can cope with situations where LDA fails. This means that our TF approach is free of the restrictive condition, prevailing for LDA, that the Cooper pair coherence length must be shorter than a typical length l (the oscillator length in the case of a harmonic container) over which the mean field varies appreciably. On the contrary, our TF theory has the usual TF validity criterion, namely that local wavelengths must be shorter than l .

The accuracy of our TF approach opens wide perspectives for a treatment of inhomogeneous superfluid Fermi-systems with a great number of particles not accessible for a quantal solution of the BCS (HFB) equations. Such systems may be cold atoms in deformed containers (eventually reaching millions of particles), superfluid-normal fluid (SN) interfaces, vortex profiles, etc. As a matter of fact, as is well known⁷, the TF approach becomes the more accurate, the larger the system. Thus the TF approximation is complementary to the quantal one in the sense that the former works where the latter is difficult or even impossible to be obtained numerically.

Ideas and part of this paper have been published in earlier works, see for instance Refs.^{36,37}. A similar semiclassical approach also has been put forward for mesoscopic systems in Ref.³⁸.

We thank K. Hagino for pointing to Ref.²⁶ and sending own results prior to publication. Special thanks are due to A. Pastore and J. Margueron for valuable discussions and ongoing collaboration on the isolated nuclei problem²⁹. B. Juliá-Díaz is gratefully acknowledged for providing us the quantal results of the double well potential. This work has been partially supported by the IN2P3-CAICYT collaboration (ACI-10-000592). One of us (X.V.) acknowledges grants FIS2008-01661 and FIS2011-24154 (Spain and FEDER), 2009SGR-1289 (Spain) and Consolider Ingenio Programme CSD2007-00042 for financial support.

References

1. L. Pitaevskii and S. Stringari, *Bose-Einstein Condensation* (Clarendon, Oxford, 2003).
2. H. Kucharek, P. Ring, P. Schuck, R. Bengtsson and M. Girod, Phys. Lett. **B216**, 249 (1989).
3. X. Viñas, P. Schuck, M. Farine and M. Centelles, Phys. Rev. **C67**, 054307 (2003); F. Barranco, P.F. Botignon, R.A. Broglia, G. Colò, P. Schuck, E. Vigezzi and X. Viñas, Phys. Rev. **C72**, 054314 (2005).
4. P. Haensel, *Neutron Stars 1: Equation of State and Structure*, (Springer-Verlag, New York, 2007).
5. D.M. Stamper-Kurn, H.-J. Miesner, A.P. Chikkatur, S. Inouye, J. Stenger and W. Ketterle, Phys. Rev. Lett. **81**, 2194 (1998).
6. S. Flügge, *Practical Quantum Mechanics*, (Springer-Verlag, Berlin, 1974).
7. P. Ring and P. Schuck, *The Nuclear Many-Body Problem*, (Springer-Verlag, Berlin, 1980).
8. L. Viverit, S. Giorgini, L.P. Pitaevskii and S. Stringari, Phys. Rev. **A63**, 033603 (2001).
9. A. Smerzi, S. Fantoni, S. Giovanazzi and S.R. Shenoy, Phys. Rev. Lett. **79**, 4950 (1997).
10. X. Viñas, P. Schuck and M. Farine, arXiv:1106.0187, J. of Phys.:Conf.Ser. **321**, 012024 (2011).
11. M. Baldo, P. Schuck and X. Viñas Phys. Lett. **B663**, 390 (2008).
12. J.W. Negele and D. Vautherin, Nucl. Phys. **207**, 298 (1973).
13. G.A. Baym, H.A. Bethe and C.J. Pethick, Nucl. Phys. **175**, 225 (1971).
14. J. Dechargé and D. Gogny, Phys. Rev. **C21**, 1568 (1980); J.-F. Berger, M. Girod and D. Gogny, Comp. Phys. Comm. **63**, 365 (1991).
15. The D1S force for pairing has been multiplied with a factor 0.85 to compensate for the use of the bare mass in the calculation.

16. M. Grasso, E. Khan, J. Margueron and N. Van Giai, Nucl. Phys. **A807**, 1 (2008).
17. M. Baldo, U. Lombardo, E.E. Saperstein and S.V. Tolokonnikov, Nucl. Phys. **A750**, 409 (2005); M. Baldo, E.E. Saperstein and S.V. Tolokonnikov, Eur. Phys. J. **A32**, 97 (2007).
18. M. Baldo, E.E. Saperstein and S.V. Tolokonnikov, Phys. Rev. **C75**, 025802 (2007).
19. A. Pastore, S. Baroni and C. Losa, Phys. Rev. **C84**, 065807 (2011).
20. F. Grill, J. Margueron and N. Sandulescu, Phys. Rev. **C84**, 065801 (2011).
21. We thank F. Grill for having sent to us the pairing energies corresponding to the calculation with the 'ISS' force in.²⁰
22. A. Pastore, F. Barranco, R.A. Broglia, and E. Vigezzi, Phys. Rev. **C78**, 024315 (2008).
23. N. Chamel, S. Goriely, J.M. Pearson and M. Onsi, Phys. Rev. **C81**, 045804 (2010).
24. I. Hamamoto, Phys. Rev. **C71**, 037302 (2005).
25. P. Schuck, X. Viñas, J. of Phys.: Conf. Series **338**, 012016 (2012).
26. N. Tajima, Eur. Phys. J. **25**, 571 (2005).
27. K. Hagino and H. Sagawa, arXiv:1105.5469
28. We thank K. Hagino for sending us his results.
29. A. Pastore et al. work in progress.
30. S. Shlomo, Nucl. Phys. **539**, 17 (1992).
31. Yu.A. Litvinov et al., Phys. Rev. Lett. **95**, 042501 (2005).
32. M.Yamagami, Y.R.Shimizu, T.Nakatsukasa, Phys. Rev. **C80**, 064301 (2009).
33. <http://www-phynu.cea.fr>
34. X. Viñas, P. Schuck and M. Farine, Int. J. Mod. Phys. **E20** 399 (2011)
35. P. Schuck and X. Viñas, work in progress.
36. M. Farine, P. Schuck and X. Viñas, Phys. Rev. **A62**, 013608 (2000); M. Farine, F.W.Hekking, P. Schuck and X. Vinas, Phys. Rev. **B68**, 024507 (2003).
37. P. Schuck and X. Viñas, Phys. Rev. Lett. **107**, 205301 (2011).
38. A.M. Garcia-Garcia, J.D. Urbina, E.A. Yusbashyan, K. Richter and B.L. Altshuler, Phys. Rev.**B83**, 014510 (2011).